A Reaction-Diffusion Transport Model to Predict Precursor Uptake and Spatial Distribution in Vapor Phase Infiltration Processes

Yi Ren[a,†], Emily K. McGuinness[b,†], Chaofan Huang[c], V. Roshan Joseph[c], Ryan P. Lively[a,*], Mark D. Losego[b,*]

[a] School of Chemical and Biomolecular Engineering, Georgia Institute of Technology, Atlanta, GA 30332, United States

[b] School of Materials Science and Engineering, Georgia Institute of Technology, Atlanta, GA 30332, United States

[c] H. Milton Stewart School of Industrial and Systems Engineering, Georgia Institute of Technology, Atlanta, GA 30332, United States

[†]These authors contributed equally to the work

Corresponding Authors: ryan.lively@chbe.gatech.edu and losego@gatech.edu

Abstract

Vapor phase infiltration (VPI) has emerged as a scalable process for transforming polymer products into a variety of organic-inorganic hybrid materials with potential applications to a number of commercial industries. However, the fundamental transport kinetics of VPI are still not well understood. Most explorations to date have relied on simple Fickian diffusion models for VPI transport. However, these Fickian diffusion models often fail to entirely capture the physical phenomena of VPI because of the complex convolution of diffusion and reaction processes. In this work, a reaction-diffusion model is developed that provides critical insight into how the presence of reactions between polymers and metal-organic precursors modifies the transport behavior of the metal-organic VPI precursor through the infiltrated polymer. From this model, parameters such as

the second order rate constant for the reaction between the precursor and polymer and a diffusive hindering factor can be extracted. The model is shown to both fit well to physical measurements and, more critically, predict experimental outcomes. Additionally, nondimensionalization is employed to create domain maps based on a wide variety of VPI parameters. The resulting domain maps showcase the breadth of behaviors captured by the reaction-diffusion model for VPI.

1. Introduction

Vapor phase infiltration exposes organic polymers to vapor-phase metal-organic precursors that sorb and diffuse throughout the polymer, eventually becoming entrapped (through reaction or loss of volatility) thus creating an organic-inorganic hybrid material.[1-6] After exposure to the metal-organic precursor, a second, vapor-phase co-reactant (e.g., water or oxygen) is delivered to react with the precursor inside of the polymer to produce a final inorganic product that is stable in ambient atmosphere. These hybrid materials have demonstrated a variety of industrially relevant properties such as increased electrical conductivity,[7-10] solvent stability,[11, 12] photoluminescence,[13-16] and enhanced mechanical properties.[17-19] Additionally, VPI can be leveraged to create high-fidelity inorganic nanostructures from sacrificial copolymer templates[20-28] and to selectively image polymer phases in polymeric mixtures with electron microscopy.[29-31] Critically, VPI is capable of forming these hybrid materials across numerous length scales and without significantly modifying the original polymer's macroscale form or microstructure.[12, 13, 32] As a result, VPI has been applied in a wide variety of fields, from polymer membranes for chemical separations to photovoltaics, catalysis, triboelectricity, gas sensing, and more. Several excellent reviews exist in the VPI field that explore the multitude of applications and opportunities for this process.[1-6]

Despite the increasing interest in VPI for its applications, the influence of VPI processing parameters on the underlying transport processes remain largely unknown. A wide range of

operational factors (e.g., vapor pressure, temperature, and polymer thickness) and intrinsic properties (e.g., density of reactive polymeric functional groups, precursor size, and precursor-polymer reaction rates) control precursor sorption and diffusion into a polymer. The complexity of these transport processes and convoluting effects of different processing parameters makes process modeling challenging and prediction of resulting hybrid material structures difficult. For VPI to emerge as a robust industrial process, a model capable of capturing these many complexities and predicting the final distribution of infiltrated inorganic species is imperative.

Within the vacuum science community, preliminary work has been done in this area with a focus on extracting fundamental parameters from experimental data. Kinetic parameters, such as diffusion coefficients, have been quantified and general trends have been observed using *in situ* experimental techniques such as quartz crystal microgravimetry (QCM),[33-37] and spectroscopic ellipsometry[38, 39] as well as *ex situ* techniques such as time of flight secondary ion mass spectrometry (TOF-SIMS),[37, 40, 41] cross-section electron microscopy paired with EDX,[42] and spectroscopic ellipsometry.[40] Additional information has also become available from these works, such as the observation of non-Fickian diffusion behavior in certain precursor-polymer systems,[33] dependency of diffusion coefficients on concentrations of reactive groups,[38] and the influence of temperature on both equilibrium sorption uptake and diffusion behaviors.[40] Recently, investigations of more thermodynamic parameters have also begun. For example, Weisbord et al. used a combination of density functional theory (DFT) and QCM experiments to determine "balance point" temperatures where forward and reverse reactions between polymers and precursors reach maximum mass uptake.[34]

While observations and some quantification of these parameters have emerged, few models have been capable of capturing the complex transport behaviors of the infiltration process. Initial studies

in VPI literature assumed purely Fickian behavior for infiltration even in systems that had clear deviations, likely due to the presence of reactions. Through a wide range of studies, it has become evident that the presence of reactions in a VPI system plays a critical and complex role in the transport kinetics of infiltration. Leng and Losego worked towards modeling systems with reactions by proposing an effective diffusion coefficient with dependency upon the reaction constant of the system.[40] While Leng's model accounts for how reaction consumes the vapor precursor it does not consider how reacted product can contribute to the precursor uptake (detailed analysis of Leng's model is provided in Section S1 in SI). Thus, an improved model for deconvoluting the influence of reactions and predicting the behaviors of varying other experimental conditions is necessary.

This work aims to build upon the work done in both the VPI and polymer sorption fields to establish a reaction-diffusion transport model that aids in the design of VPI processes for desired inorganic loading and serves as a theoretical reference to compare with experiments. Importantly, we demonstrate for the first time a model that deconvolutes the Fickian diffusion and reaction contributions to the VPI sorption process. The capabilities of this new reaction-diffusion transport model are highlighted by validating it against experimental processes and then using it to predict the results of VPI experiments using similar chemistries but different process conditions.

2. Experimental

2.1 Quartz crystal microgravimetry (QCM): QCM experiments were used to validate the proposed model. In this work, RC cut quartz crystals of approximately 6 MHz operating frequency were used (see table S2 for exact frequency values). RC crystals were used for their decreased noise in processes at higher operating temperatures. Shifts in the crystal's frequency were converted to

mass per area using the Sauerbrey equation and normalized to the mass per area of polymer on the crystal. A description of the data processing is included in Section S8 of the SI.

Poly(methyl methacrylate) films [Polysciences Inc., 75K molecular weight] were spun cast (3000 rpm, 60 seconds) onto the crystals from approximately 2 mL of 10 wt% solutions of PMMA in toluene (anhydrous, 99.8%, Sigma-Aldrich). Films near the edge of the crystal were removed with a cotton swab soaked in toluene to allow frontside contact to the microgravimeter. These films had a nominal thickness of 500-600 nm. Immediately prior to infiltration, the crystals were heated to 150˚C for 1 hour on a hotplate in air to remove any processing history. Frequency shifts due to the polymer loading were measured and checked to make sure the change in frequency was less than five percent to avoid violating the Sauerbrey equation.

2.2 Vapor phase infiltration (VPI): Microgravimetry was conducted in a hot-walled custom designed VPI reactor using the Phoenix™ System with Eon-LT™ Monitor from Colnatec. The films were then infiltrated at 130˚C with trimethylaluminum (TMA, **DANGER:** Pyrophoric, Strem Chemicals, 98%, TMA source bottle kept at room temperature) and co-reacted with water vapor dosed from a glass container (DI Water, room temperature). The VPI process was conducted using custom-designed Labview tree-based software to control pneumatic valves on the reactor and pressure values were monitored and reported via a Baratron capacitance manometer.[43] The first step in the VPI process was a one-hour nitrogen purge (On Site Gas Systems, < 10 ppm O_2) followed by 17.5 hours of active pumping at rough vacuum (~30 mTorr) to remove sorbed water and residual solvents. The reactor was then isolated and TMA was dosed into this static environment to either 8.7 or 10.5 Torr of TMA pressure (see pressure profiles for all experiments in Section S9). The reactor was left in this state for 17.5 hours and then underwent another 17.5 hours of active pumping. The reactor was isolated once more and water vapor introduced at

approximately 17.8 Torr of pressure. The reactor was left isolated in this state for 17.5 hours and then a final 17.5 hour active pumping step was performed. The final step before removal was a 2 to 3 hour nitrogen purge. Temperature of the reactor walls was controlled via a custom PID control system and the QCM temperature was controlled using the Mirage Air Cooling System by Colnatec.

2.3 Spectroscopic Ellipsometry: Ellipsometry was used to measure film thickness of the polymer before infiltration and the hybrid material following infiltration. Measurements were taken on a J.A. Woollam Alpha SE from 500 to 900 nm. Data was fit using a Cauchy model. All fits had mean square errors of less than 30.

3. Reaction-Diffusion Transport Model Development

For a VPI process, the metal-organic precursor may occupy one of at least two different states within the polymer. It may be physically sorbed within the polymer or chemically sorbed to (e.g., reacted with) functional groups within the polymer. For VPI chemistries in which precursors are only physically sorbed and induce little change to the polymer (e.g. no plasticization), Fickian models should be sufficient for capturing the salient features of infiltration. However, for systems in which the precursor can both physically and chemically sorb, the requisite transport model must mathematically account for both the diffusion kinetics as well as the chemical reaction kinetics.

3.1 Fickian Transport

For Fickian diffusion of vapors into polymers, the molecular penetrant is assumed to have no significant interactions with the polymer, i.e., no chemical reactions, no swelling, and no changes to the polymer's properties. The use of Fickian diffusion to model VPI transport may be suitable for certain VPI systems where reactions do not occur between the penetrants and the polymer

backbone and material properties remain constant with processing time. Several works in the infiltration community have used Fickian diffusion to approximate transport behaviors, especially under short precursor exposures.[33, 44] For completeness, a Fickian solution applicable to VPI in systems without reactions or swelling is provided in Section S2 of the supporting information.

3.2 Assumptions for a Reaction-Diffusion Transport Model for VPI

In many VPI systems, chemical reactions occur between the penetrant precursors and the polymer's functional groups. In these systems, the reacted immobilized products fill polymer free volume and create barriers to diffusion, reducing the diffusion coefficient as a function of process time. An example of this behavior is seen in work by Sinha et al. where for reactive infiltration process such as $TiCl_4$ with PMMA, the diffusivity decreases as $TiCl_4$ infiltrates into the polymer, and the precursor uptake curve deviates away from the pure Fickian diffusion model.[45] To account for these time dependencies, we propose a reaction-diffusion transport model that attempts to capture temporal changes in diffusivity through a set of differential equations representing changes in polymer free volume due to an irreversible second-order reaction.

The main assumptions of the reaction-diffusion model are illustrated in Figure 1. The polymer's geometry is assumed to be an infinite sheet with thickness 2ℓ, which remains constant with respect to time. Assuming a constant thickness is a major assumption and is discussed at length in the model limitations section. This sheet is infiltrated by precursors from both sides resulting in a characteristic length of ℓ. The polymer volume is assumed to be infinitely smaller than the reactor volume such that the external vapor pressure of the precursor remains constant with time. Immediately upon introduction of the metal-organic vapor an equilibrium is established between the fixed vapor pressure and the polymer surface. This surface concentration is estimated via Henry's Law (Figure 1a). The use of a linear sorption isotherm (Henry's law) is a major

assumption and may be improved upon in the future when more information regarding the sorption isotherms in VPI is made available. During the precursor exposure step of VPI (Figure 1a-c) the precursor diffuses within the polymer and reactions occur. It is assumed that once a precursor molecule diffuses away from the surface, a new precursor molecule immediately replaces it from the overpressure such that there is a constant surface concentration (C_s). As reactions take place, the immobilized product takes up local free volume, decreasing the local diffusion coefficient. Thus, during precursor exposure, both free diffusing precursor and reacted product co-exist in the polymer, both contributing to the mass uptake. For this model, the reactions are assumed to be second order and irreversible with an order of one for both precursor concentration and reactive polymer functional group concentration. It is assumed that no byproducts are created as a result of this process (which is often not true).

In most VPI processes, the precursor exposure step is sequentially followed by the removal of the precursor overpressure (either through a continuous nitrogen purge or active pumping), that accordingly brings the surface concentration to zero. Due to the change in chemical potential, free-diffusing precursors will diffuse out of the polymer, while immobilized product will remain trapped in the polymer as depicted in Figure 1d. This desorption step can vary in length, but given sufficient time, this step can provide key information regarding the quantity of immobilized precursor within the polymer. Therefore, the model developed here includes an analysis of the desorption process. The overall VPI process is assumed to be isothermal, with no polymer swelling or relaxation taken into consideration. A detailed explanation of the reaction-diffusion model's assumptions is provided in Section S3.

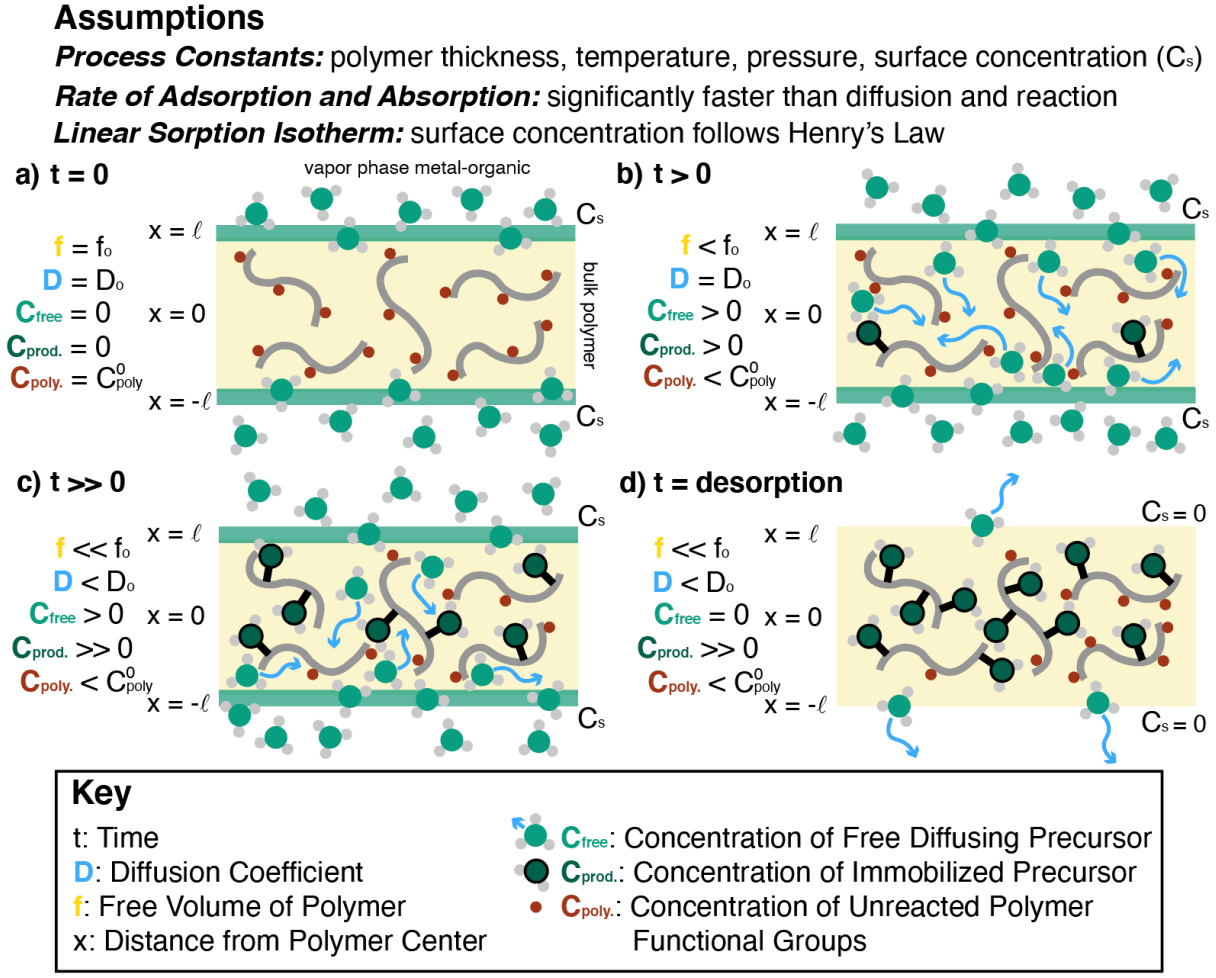

Figure 1. *Illustration of a VPI process that includes reactions between the polymer and metal-organic precursor. a) Metal-organic vapor is introduced into the system and instant equilibrium between polymer surface and vapor pressure is obtained. b) The precursor penetrant starts to diffuse into the polymer bulk. Some penetrant molecules react with the polymer functional groups and become immobilized (dark green). c) As time progresses, more and more freely diffusing precursor reacts with the polymer, creating higher concentrations of immobilized product. Both freely diffusing and immobilized precursors contribute to the total inorganic uptake. d) As a desorption step is applied, freely diffusing penetrant molecules desorb back to the vapor phase and get removed. Immobilized precursor remains.*

3.3 Governing Equations of the Reaction-Diffusion Transport Model for VPI

The following set of equations are proposed to model the reaction-diffusion transport phenomena in a VPI process that includes irreversible second-order reactions and a temporal change in diffusivity:

$$\frac{\partial C_{free}}{\partial t} = D\frac{\partial^2 C_{free}}{\partial x^2} - k \cdot C_{free} \cdot C_{polymer} \quad (1)$$

$$\frac{\partial C_{product}}{\partial t} = k \cdot C_{free} \cdot C_{polymer} \quad (2)$$

$$D = D_0 \exp(-K' \cdot C_{product}) \quad (3)$$

$$\frac{\partial C_{polymer}}{\partial t} = -k \cdot C_{free} \cdot C_{polymer} \quad (4)$$

where C_{free} (mol/cm^3) is the concentration of free diffusing vapor, k (cm^3/mol•s) is the reaction rate constant of a second-order reaction, $C_{polymer}$ (mol/cm^3) is the concentration of the accessible reactive polymeric functional groups, $C_{product}$ (mol/cm^3) is the concentration of the immobilized product, D_0 (cm^2/s) is the initial diffusivity of the precursor into the fresh polymer, and K' (cm^3/mol) is a hindering constant related to the free volume of the polymer and the molecular size of the penetrant.

Eqn. 1 combines Fick's 2nd law with a reaction term to describe the process in which the free diffusing precursor diffuses through the polymer film while being consumed by reaction. Eqn. 2 accounts for the rate of formation of the immobilized product. Eqn. 3 (the hindering equation) assumes that diffusivity decreases exponentially with $C_{product}$, which aligns with the semi-empirical model proposed by Thornton et al. to predict the diffusivity of gas permeating into a polymer, based on the free volume of the polymer (Equation 5). The model proposed by Thornton et al. was shown to be an improvement over the widely known Dolittle relation, viz.,

$$D = \alpha \exp(\beta f) \quad (5)$$

where f is the free volume, and α and β are constants fitted empirically. In the reaction-diffusion model proposed here it is assumed that the free volume decreases linearly with the concentration of immobilized product such that $f = f_0 - \frac{K'}{\beta} \cdot S$.[46] Thus Eqn. 3 and Eqn. 5 are in the same form. Finally, Eqn. 4 captures the rate at which accessible reactive polymer functional groups are consumed.

The initial and boundary conditions for the governing equations of VPI sorption and desorption are provided in S4. In the proposed model, six parameters are included that are known to influence the VPI process: polymer thickness 2ℓ (cm), initial density of the polymer's reactive and accessible functional groups $C^0_{polymer}$ (mol/cm^3), equilibrium surface concentration of sorbed precursors C_s (mol/cm^3), which is related to the process vapor pressure via Henry's law, fresh polymer diffusivity D_0, the reaction rate constant k, and the hindering constant K', which is designed to capture the reduction in diffusivity due to the reaction between precursor and polymer.

3.4 Non-dimensionalization of the Reaction-Diffusion Model

It is challenging to analyze the VPI process systematically; indeed, the proposed reaction-diffusion model utilizes six parameters that influence the VPI process. Dimensionless values can be used to reduce the complexity of the problem into small collections of important parameters. The dimensionless variables for the reaction-diffusion model are as follows:

$$X = \frac{x}{\ell} \tag{6}$$

$$\tau = \frac{Dt}{\ell^2} \tag{7}$$

$$\varphi = \frac{C_{free}}{C_s} \quad (8)$$

$$C_{polymer} = C^0_{Polymer}(1 - \varepsilon) \quad (9)$$

where $C_{polymer}$ is defined by a constant and a unitless parameter ε, which is the extent of reaction (the extent to which the reaction proceeds). By using the dimensionless length, time, and concentration parameters, the VPI model (Eqn.1 to Eqn.4) can be modified as shown:

$$\frac{\partial \varphi}{\partial \tau} = \frac{\partial^2 \varphi}{\partial X^2} - k\frac{\ell^2}{D} \cdot C^0_{Polymer} \cdot \varphi \cdot (1 - \varepsilon) \quad (10)$$

$$\frac{\partial \varepsilon}{\partial \tau} = Da\,(1 - \varepsilon) \cdot \varphi \cdot \frac{C_s}{C^0_{Polymer}} \quad (11)$$

$$\frac{D}{D_0} = \exp(-K' \cdot C^0_{Polymer} \cdot \varepsilon) \quad (12)$$

The following coupled numbers form a dimensionless set that can describe the system entirely.

$$k\frac{\ell^2}{D_0} \cdot C^0_{Polymer} = Da \quad (13)$$

$$\frac{C_s}{C^0_{Polymer}} \quad (14)$$

$$K' \cdot C^0_{Polymer} \quad (15)$$

Eqn. 13 is the second-order Damkohler number Da (illustrated in Figure 2a), which is used to describe the ratio of reaction rate to diffusion rate, and is commonly used in transport kinetics.[47,

[48] Da has also previously been utilized to study ALD and CVD transport in the vacuum science community.[49] If Da >>1, the reaction rate is much faster than diffusion rate indicating the process is diffusion-limited, and if Da <<1 the diffusion rate is much faster and the process is reaction-limited.

Eqn. 14 is the ratio of vapor surface concentration to initial accessible reactive polymer functional group concentration and is illustrated in Figure 2b. Since surface sorption is assumed to be immediate, the main controlling parameter of surface concentration is the precursor pressure while $C^0_{Polymer}$ will depend upon the chemical structure of the polymer and the precursor. The ratio of $C_s/C^0_{Polymer}$ will also dictate the theoretical values of free diffusing to immobilized species, and the total precursor uptake that can be contributed by both.

Finally, Eqn. 15 (Figure 2c) represents the hindering degree created by the immobilized precursor. Since the diffusion hindering process could be related to both the polymer-precursor property (i.e., the fractional free volume of polymer and molecular size of precursor represented by K') and the concentration of reactive and accessible functional groups (represented by $C^0_{Polymer}$), the coupled hindering number $K' \cdot C^0_{Polymer}$ combines both and describes the decrease in the diffusion rate upon the creation of immobilized precursors.

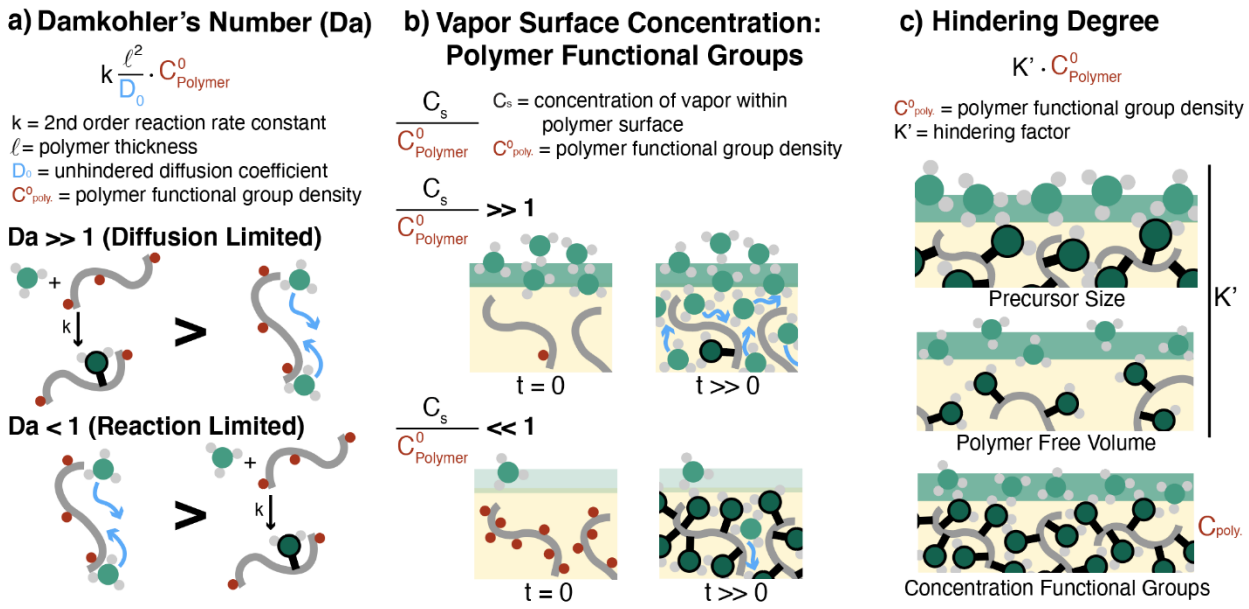

Figure 2. *Illustrations of the dimensionless number set proposed to fully describe the VPI systems with reactions. a) Damkohler number b) ratio of the concentration of vapor within the polymer surface to reactive and accessible polymer functional groups c) hindering degree (dependent on multiple parameters such as precursor size, polymer free volume, and concentration of reactive polymer functional groups).*

4. Results and Discussion

4.1 Domain Mapping Using Dimensionless Numbers in the Reaction-Diffusion Model

Dimensionless numbers help to explain the convolution of various process parameters and how seemingly dissimilar values of process parameters can lead to the same experimental output. For example, Figure S5 illustrates the dimensionless plotting of pure Fickian kinetics and how identical process outcomes are achieved with different process conditions so long as these conditions lead to the same set of dimensionless numbers.

To visualize the dimensionless numbers of the reaction-diffusion model, we create process domain maps illustrating mass uptake as a function of the three dimensionless numbers identified above. Figure S6 demonstrates that these domain maps are the same for various combinations of the original six process parameters as long as the dimensionless set remains identical.

To explore how well the dimensionless numbers of the reaction-diffusion transport model represent the types of precursor uptake behaviors observed in VPI, we consider 45 scenarios in Figure 3 with three concentration ratios of $\frac{C_s}{C^0_{Polymer}}$ (0.1, 1, and 10), three hindering degrees $K' \cdot C^0_{Polymer}$ (0.5, 5, 50), and five different D_a ranging from 0.01 to 100, increasing by a factor of 10.

For $\frac{C_s}{C^0_{Polymer}}$, a value of 0.1 and below indicates a low surface concentration in relation to the concentration of accessible and reactive polymer functional groups. A low value can arise from a variety of phenomena such as low precursor vapor pressure, limited precursor solubility within the polymer, or simply a high concentration of accessible and reactive polymer functional groups. High values of $\frac{C_s}{C^0_{Polymer}}$ represent the opposite conditions. For $K' \cdot C^0_{Polymer}$, a value of 0.5 and below represents low to negligible hindering effects, i.e. diffusion will change little with product formation, while a value of 50 indicates significant hindering which might result in the formation of an impermeable layer. Finally, the range of Da is from 0.01 to 100 following conventional ranges for models involving Damkohler number.

For illustrative purposes, desorption is arbitrarily chosen to take place in Figure 3 at the dimensionless "time" interval of $\sqrt{D_0 t/\ell^2} = 16$. At this interval penetrants that are Fickian in nature have had "excessive" amounts of time to diffuse into the polymer (an average diffusion length that is 16x the polymer's thickness assuming a relative random walk Fickian model). All precursor uptake curves are normalized to M_∞ (the theoretical maximum of precursor uptake that could be reached before desorption occurs). Details of the definition of M_∞ can be found in S7. Since the film is modeled as an infinite film with finite thickness, M_t and M_∞ are the area

normalized mass (mass per surface area), and are obtained by integrating local concentration over the film thickness.

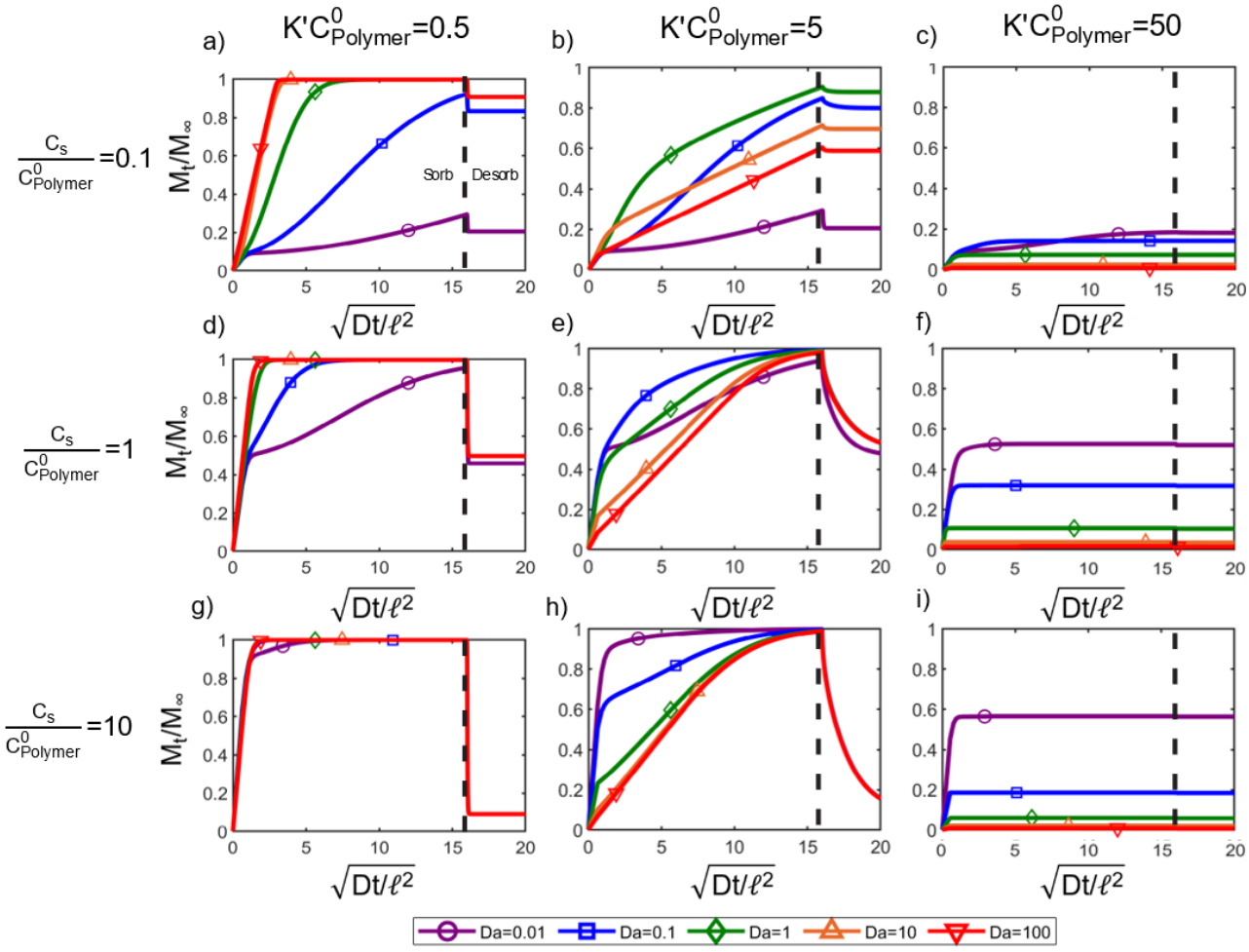

Figure 3. *Dimensionless mapping for all VPI scenarios defined by* $\frac{C_s}{C^0_{polymer}}$, $K'C^0_{Polymer}$, *and* Da, *color legend represents* Da

Figure 3a-i plots the reaction-diffusion transport model calculations for the VPI mass uptake as a function of different combinations of these three dimensionless numbers. These computations illustrate that the reaction-diffusion transport model can capture many of VPI phenomena observed in literature. Here we highlight some of these phenomena.

First, consider the dimensionless number $C_s/C^0_{Polymer}$, which represents the ratio of the concentration of precursor at the polymer surface to the concentration of accessible reactive functional group sites in the polymer. The influence of this parameter alone on mass uptake behaviors is best illustrated under low hindering conditions with high Damkohler numbers (Figure 3 a, d, g). As $C_s/C^0_{Polymer}$ increases (down the column) the relative amount of mass retained after desorption decreases. During the sorption step, precursors diffuse throughout the polymer's bulk and this concentration of "free diffusing" precursors will approach the surface concentration (C_s). In a system with reactions, some of these free diffusing species will react and become immobilized and be replaced with additional free diffusing species from the precursor overpressure. Once equilibrium is reached, the ratio ($C_s/C^0_{Polymer}$) becomes the relative ratio of free diffusing species to immobilized species in the polymer. Subsequently upon desorption, the free diffusing species are removed from the bulk. As a result systems with higher $C_s/C^0_{Polymer}$ ratios will have lower relative concentrations of immobilized species and show more total metal-organic mass loss during the desorption step. This result describes observations in experimental systems well (*vide infra,* Figure 5) where for the same polymer (constant $C^0_{Polymer}$) experiments with higher precursor pressures (and therefore higher C_s) result in greater precursor uptake during the precursor sorption step, but the same precursor uptake for lower pressure experiments following the desorption step. Additionally, for VPI systems with identical $C_s/C^0_{Polymer}$ values that reach saturation under low hindering conditions (Figure 3 a, d, g) both the retained mass and desorption kinetics will be the same regardless of the sorption kinetics. This is shown by the identical desorption curves for these modeled systems at the same $C_s/C^0_{Polymer}$.

Next, consider the Damkohler number (*Da*), which is represented by the different curves in each graph of Figure 3. A higher *Da* indicates a diffusion-limited process (fast reactions) while a lower *Da* indicates a reaction-limited process (fast diffusion). To a first order, one may think that as the Damkohler number increases (reaction rates increase), transport will be slower and it will take longer during the sorption step to reach saturation ($M_t/M_\infty = 1$). In some instances, this occurs such as in Figure 3h when $C_s/C^0_{Polymer}$ is high and the hindering of the reacted species is significant. However, a complex interplay exists between $C_s/C^0_{Polymer}$ and the Damkohler number. For example, Figure 3a shows the opposite trend in saturation time as a function of Damkohler number. In fact, the lowest *Da* (reaction-limited) does not reach saturation during the modeled timeframe. Under these conditions where $C_s/C^0_{Polymer}$ is low, the reacted portion contributes more to the total mass uptake than the free diffusing species. Therefore, the time to saturation depends more strongly on the reaction rate than the diffusion rate and the resulting curves reflect this dependency. Comparing *Da* = 0.01 in Figure 3a with Figure 3g, it is evident that this model captures how reaction-limitations play a less dominant role in systems where free diffusing species greatly outnumber immobilized species.

Finally, if the immobilized precursors alter the inherent diffusivity of the material, then a "hindrance" effect may be observed. Each column of Figure 3 depicts an increase in hindrance ($K' \cdot C^0_{Polymer}$) from left to right. In all cases (looking from plots left to right), we see a suppression of the time to saturation and eventually an effective suppression of the saturation value during the modeled timeframe ($M_t/M_\infty < 1$). For the most extreme hindering conditions (right most column, $K' \cdot C^0_{Polymer} = 50$), equilibrium saturation is never achieved and only a fraction of the polymer is ever infiltrated. The severely reduced diffusivity of the infiltrated material creates what has been described in the literature as an "impermeable barrier" to further diffusion. Under these conditions,

desorption will also be similarly blocked as out-diffusion cannot occur through this impermeable layer. In this way, the model presented here captures the transition from VPI behavior to a self-limiting surface coating behavior similar to atomic layer deposition (ALD). This type of surface coating behavior has been seen experimentally in vapor phase treatments of polymers such as cellulose, poly(vinyl alcohol), and poly(acrylic acid), which possess high concentrations of reactive functional groups.[36, 50-59]

Interestingly, in the most hindered model conditions ($K' \cdot C^0_{Polymer} = 50$, Figure 3c, f, i), a higher Da (faster reactions) results in lower precursor uptake, which is the opposite observation from the least hindered cases (Figure 3a, d, g). This observation reflects the model's ability to physically represent how systems with more diffusion-limited (faster reaction rate) will form an impermeable layer faster, while reaction-limited systems can permit more precursor infiltration before diffusion is prohibited. Depth profile analysis in the next section will further support this predicted phenomenon.

In systems with moderate hindering (Figure 3b, e, and h) the complex interplay between *Da* and $C_s/C^0_{Polymer}$ is most evident with the time to saturation depending strongly on the combination of these parameters. In Figures 3h, the lowest *Da* values (slow reaction rates) result in the fastest uptake because the free diffusing precursors (which account for the majority of the mass uptake according to $C_s/C^0_{Polymer}$) are able to reach saturation before a significant quantity of species become immobilized and hinder diffusion. Moving to Figures 3b and e, where the $C_s/C^0_{Polymer}$ is low or balanced, moderate *Da*'s exhibit the fastest time to saturation as the free diffusing species enter relatively quickly before hindering becomes significant and the reactions proceed rapidly enough to not delay the mass uptake due to sorption. An example of this may be seen in the

infiltration of TMA into PMMA reported by Dandley et al., [60] where initial mass uptake is relatively fast at temperatures of 100ºC and 140˚C. However, as time increases, the mass uptake at 140˚C slows in comparison to that of 100˚C,[60] likely due to a higher reaction rate and therefore a higher *Da*. As a moderately hindered system, this higher *Da* leads to a slower approach to equilibrium as more of the free diffusing species have to navigate a more tortuous environment. While it is challenging to quantitatively fit the model to this experimental data because it lacks a prolonged, single-exposure step, the experimentally reported phenomena qualitatively matches the model predictions.

4.2 Depth Profiles Generated Using the Reaction-Diffusion Model

In addition to understanding the VPI process through mass uptake, it is worthwhile to investigate how infiltrated precursors are distributed throughout the depth of the polymer. Depth profiles are frequently created experimentally in the VPI community to help increase understanding of VPI processes.[40-42] Additionally, the distribution of inorganic throughout the bulk of the polymer can play a role in material properties such as solvent stability.[11] This section will show that the reaction-diffusion transport model can also create depth profiles to enhance understanding of VPI kinetics.

Figure 4 plots depth profiles calculated from the reaction-diffusion transport model to show the spatial distribution of precursors throughout the film's thickness as a function of time. Four combinations of low *Da*, high *Da*, low hindering, and high hindering are plotted at fixed $C_s/C^0_{Polymer}$ of 0.1 for varying infiltration times between $\sqrt{D_o t/\ell^2}$ of 0.2 and $\sqrt{D_o t/\ell^2}$ of 160.

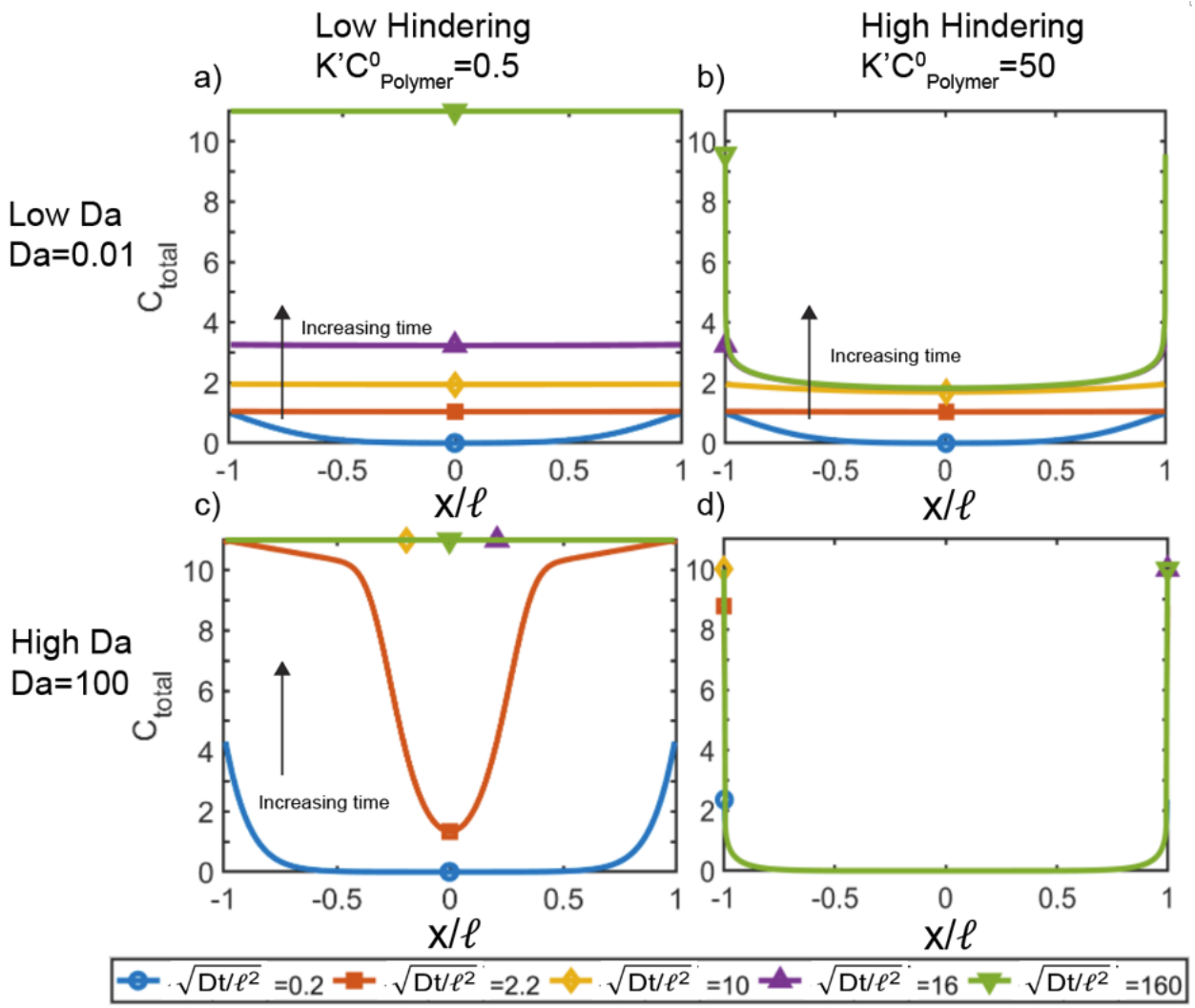

Figure. 4. *Concentration depth profiles for* $C_s/C^0_{Polymer}$ *=0.1 at varying time points* ($\sqrt{D_o t/\ell^2}$). *a) Low Da=0.01 and low hindering* $K' \cdot C^0_{Polymer}$ *=0.5 b) Low Da=0.01 and high hindering* $K' \cdot C^0_{Polymer}$ *=50 c) High Da=100 and low hindering* $K' \cdot C^0_{Polymer}$ *=0.5 d) High Da=100 and high hindering* $K' \cdot C^0_{Polymer}$ *=50. Note: a and c represent the purple and red curves respectively in Figure.3a, while b and d represent the purple and red curves in Fig. 3c.* $\sqrt{D_0 t/\ell^2}$ *=160 is simulated for sorption to show the final theoretical equilibrium uptake assuming time has gone to infinity.*

To achieve $C_s/C^0_{Polymer}$ = 0.1, C_s is chosen to be 1, and $C^0_{Polymer}$ is chosen to be 10. Therefore the theoretical maximum value for the total concentration is the sum of both, which is 11. For Figure. 4a, low *Da* (*Da*=0.01) with low hindering ($K' \cdot C^0_{Polymer} = 0.5$) is simulated. Due to the low *Da*, reactions are significantly slower than diffusion, thus a constant precursor concentration

is achieved throughout the polymer film at short infiltration times ($\sqrt{D_o t/\ell^2} = 2.2$). Slow reaction then occurs, resulting in a homogeneous increase of mass uptake. On the other hand, in Fig. 4c, since *Da*=100, reactions are significantly faster than diffusion. It is observed that mass uptake starts to build up quickly near the surface due to fast reaction rate, and concentration in the middle is lower initially due to the slow diffusion ($\sqrt{D_o t/\ell^2}$ =2.2). An example of this from literature is found in the depth profile for a diffusion limited VPI infiltration process of TMA into a thick, dense PIM-1 film that has not reached equilibrium. The inorganic content within the cross section of the film is similar to Figure 4c when $\sqrt{D_o t/\ell^2}$ =2.2, with high saturated concentration at both sides and low concentration in the middle.[12] Comparing Fig. 4a and Fig. 4c, C_{total} =11 is achieved throughout the film using a much shorter time for Fig. 4c compared to Fig. 4a due to the combination of fast reactions and low hindering.

For high hindering scenarios (right column), interesting diffusion kinetics can be observed. For Figure. 4b, low *Da* results in a slow reaction rate, which results in a homogeneous distribution of mass uptake at the initial stage when $\sqrt{D_o t/\ell^2} = 2.2$. As the concentration keeps growing and polymer film reaches a homogeneous concentration of C_{total} around 2 throughout the film, an impermeable hybridized block is gradually formed, and further diffusion is prohibited. As a result, mass only starts to grow on the surface that results in negligible change in the overall mass. For Figure 4d, high *Da* results in instantaneous reaction at the surface, and extremely high concentration is achieved at initial stage, but only at the surface due to the instantaneous high hindering effect. As time goes on, only the surface concentration is rapidly increasing, but no infiltration can occur within the bulk. Depth profiles of this nature have been observed for the infiltration of polyamide 6 (polycaprolactam) with TMA where the limited depth of the infiltrated portion decreases with higher temperature. The limited depth of infiltration may be a result of

faster reaction kinetics combined with slower diffusion due to the semi-crystalline nature of the polymer.[37]

By comparing Figures 4a and 4c, it can be concluded that at low hindering conditions, a high reaction rate can be beneficial for mass uptake rate. In contrast, Figures 4b and 4d show that, for high hindering conditions, fast reaction rates block diffusion and are detrimental for mass uptake growth whereas a slower reaction rate can allow infiltration of precursors before diffusion is prohibited. Figures 3 and 4 demonstrate how the reaction-diffusion model can be used to explain the mixed effects of reactions observed in literature, where in some conditions fast reactions aid infiltration uptake and precursor distribution throughout the polymer and in other conditions slow the infiltration.

4.3 Model Validation

The goal of this reaction-diffusion model is to (1) gain useful parameter information of elementary VPI steps and (2) predict VPI behavior (mass loading, infiltration depth, and desorption rates) based on an understanding of process chemistry and operating conditions. In this section, the practical details of obtaining each parameter will be briefly outlined for an experimental data set and then used to predict another experiment. Finally, the model will be compared with other commonly used models for small molecule transport in polymers.

One of the main challenges in building a transport model for VPI processes is the lack of standardized literature data on the key parameters. Here we describe a method for obtaining 5 out of the 6 parameters from experimental data. The one remaining parameter, reaction coefficient k, as a single degree of freedom, is estimated from the fitted data. Note that to model an infiltration system that is on a solid substrate rather than infiltrating from two sides, the characteristic length

ℓ is now the entire film thickness and the total mass uptake obtained by using Eqn. 1-4 should be halved (since the mass obtained by using Eqn. 1-4 is doubled with thickness of 2ℓ)). A detailed description of the boundary condition is provided in S14. The presence of a substrate has been shown to influence infiltration in some systems especially those with multiple alternating cycles of precursor and oxidant.[41] This may be due to physical differences in the polymer at the interface or chemical reactions that occur between the precursors and the substrate. However, in other infiltration systems the substrate is not observed to have a significant influence on the spatial distribution or overall uptake of the inorganic.[19, 31, 37, 39] For this work, the influence of substrate is assumed to be negligible.

Figure 5 plots experimental QCM mass change data for TMA sorption (Figure 5a, c) and desorption (Figure 5b, d) into a PMMA film at 130 ˚C for both 8.7 and 10.5 Torr of TMA pressure (full VPI experiments and pressure profiles are provided in Figure S9). At 130˚C, infiltration is performed above the glass transition temperature for PMMA where any swelling of the polymer is thought to be rapid and therefore not a kinetic limitation. Additionally, the reaction of TMA with the carbonyl functional groups of PMMA at this temperature is documented to proceed through a metastable intermediate and result in the formation of an irreversible covalent bond.[60-62]

The experimental data in Figure 5 exhibits several non-Fickian behaviors. The first is the deviation from Fickian diffusion at the early stages of precursor sorption. Secondly, after initial rapid precursor uptake, saturation is approached slowly. The non-Fickian nature is further evidenced by a ~700 times slower diffusion coefficient for desorption compared with sorption. These observations confirm that a Fickian model is not appropriate for this dataset.

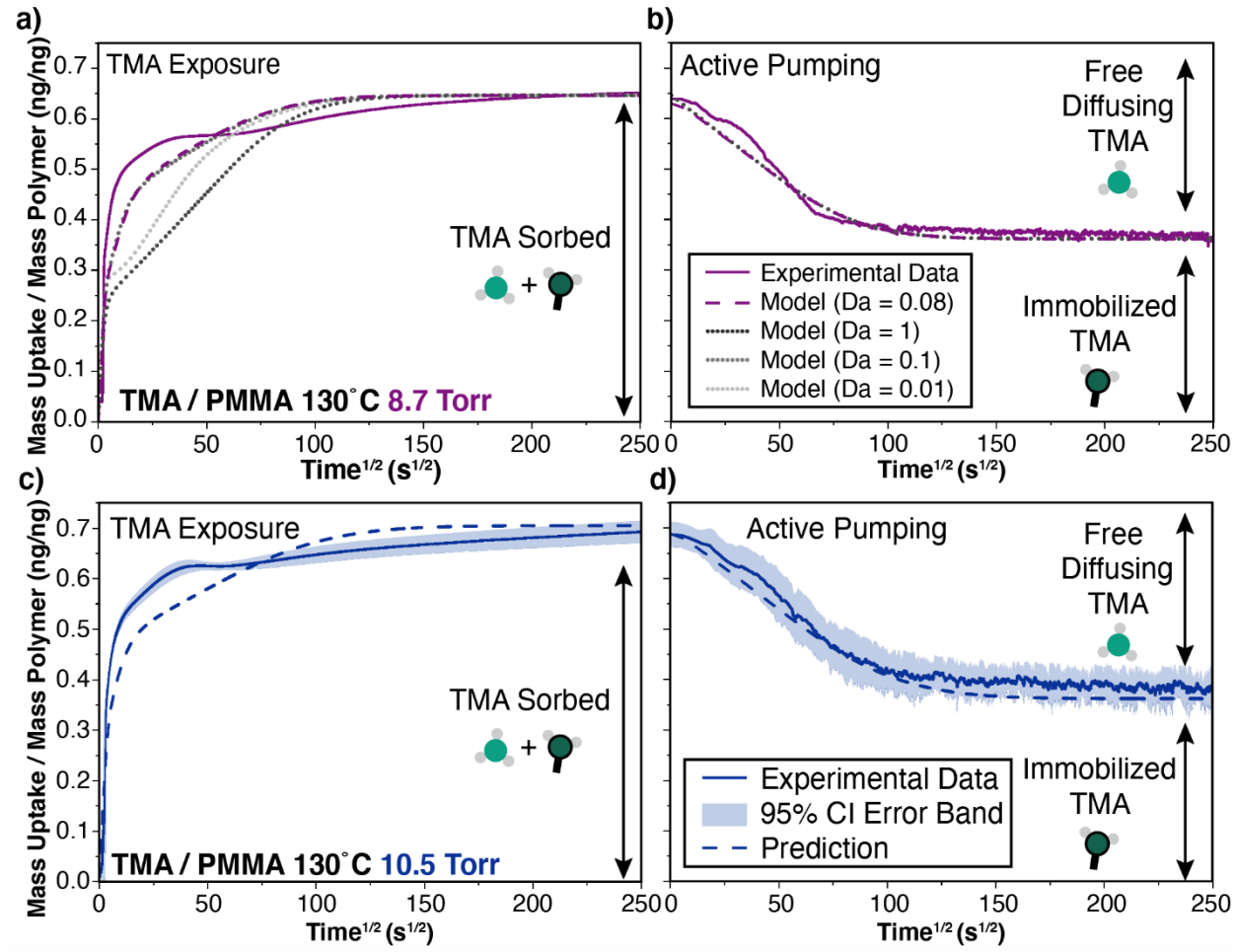

Fig 5. *Experimental QCM data for TMA sorption and desorption into PMMA thin films at 130 °C showing mass change normalized to polymer mass as a function of* $t^{1/2}$. *a) TMA sorption and b) desorption data (solid line) and model fit (dotted purple line) for VPI performed at a pressure of 8.7 Torr TMA. Included are modeled curves for varying Damkohler number (dotted gray lines) used to compare with model fit. c) TMA sorption and d) desorption data (solid line) and model prediction (dotted line) for VPI performed at a pressure of 10.5 Torr TMA. Blue shading around the 10.5 Torr experimental data represents the 95% confidence interval as determined by three experimental replicates. Sorption and desorption data are plotted in two separate figures with their own zero times to make them comparable and not distort desorption data due to the abscissa being plotted in root time.*

Table 1. Parameters extracted from 8.7 Torr TMA run and then predicted for 10.5 Torr TMA run.

	Data extracted from 8.7 Torr	Data for 10.5 Torr prediction
Thickness l (nm)	483	607
D_0 (cm^2/s)	1.65×10^{-10}	1.65×10^{-10}

C_s (mol/cm^3)	4.436x10^{-3}	5.35 x10^{-3}
$C^0_{polymer}$ (mol/cm^3)	5.656 x10^{-3}	5.656 x10^{-3}
K' (cm^3/mol)	1150	1150
k (cm^3/mol • s)	1	1

The 8.7 Torr TMA data (Figure 5a, b) is subsequently parameterized to the reaction-diffusion model for the 130 °C TMA-PMMA VPI process. The corresponding parameters are shown in Table 1. The thickness parameter is measured directly using spectroscopic ellipsometry, while the parameters of D_0, C_s, $C^0_{polymer}$, and K' are extracted from the QCM data as described in the supporting information Section S10. D_0 is obtained from the early portion of the sorption curve, C_s is obtained from the maximum mass uptake of the sorption curve, $C^0_{polymer}$ is obtained from the residual mass uptake of the desorption curve, and K' is obtained from the slope of the desorption curve. The final parameter, the reaction rate constant of a second-order irreversible reaction is determined by fitting the model using the previous five parameters and varying the Damkohler number. (Best fit was determined to be k = 1 cm^3 mol^{-1} s^{-1} , which results in *Da*=0.08. Other *Da* values are shown as dotted gray lines in Figure 5a and b for comparison.) The resulting model output (dashed purple line) qualitatively describes the VPI sorption behavior well, and fits desorption even better. The model has an overall normalized mean absolute error (nMAE) of 2.4%, with the sorption process having a nMAE of 2.7% and desorption a nMAE of 2.1%. Details of the nMAE computing are available in S13. The model's fit is less accurate during the initial sorption stage, possibly due to the model's assumption of an isothermal process and thus inability to account for the exothermic sorption phenomena that likely accelerates the initial diffusion kinetics. Another explanation could be swelling of the polymer that is not accounted for by the model.

We next use the parameters from this 8.7 Torr TMA run to predict mass change for a VPI process at 10.5 Torr TMA, 607 nm PMMA film thickness, and 130 °C process temperature. Using a Henry's Law linear isotherm to estimate the new surface concentration, we calculate the mass change for this 10.5 Torr TMA process and plot this prediction as dotted lines in Figure 5c, d. Due to the slight difference in the films' surface area, a correction factor is also used to account for the small surface area discrepancy, detailed in Section S10. The experimental data in Figure 5c, d (solid line with a 95% confidence interval band) represents QCM data collected over three separate experimental runs using these conditions. These results demonstrate the reaction-diffusion transport model's ability to accurately predict mass changes in the VPI process. These predictions have an overall nMAE of 4.4%, with a nMAE of 4.7% for the sorption process and a nMAE of 4.1% for the desorption process. While the nMAE of prediction for 10.5 Torr is slightly higher than that of fitting for 8.7 Torr, both nMAE are still in the 5% error range. This validation of the model suggests that with one VPI experiment, future experiments for the same precursor-polymer system can be anticipated computationally. Moreover, this approach enables extraction of rate parameters of elementary steps in the VPI process (e.g., D_0, C_s, $C^0_{polymer}$, k and K') that can be compared across different systems to give new insights into chemical design.

The non-dimensionalized parameters for the specific run of TMA into PMMA at 130 ºC and 8.7 Torr are also included in Section S12 for future reference.

4.4 Model Comparison

Figure 6 compares how different models, such as Fickian kinetics, Berens-Hopfenberg (which accounts for polymer relaxation and swelling through non-physical fitting parameters),[63, 64] and the newly developed reaction-diffusion model, can be fit to the experimental data for the 8.7 Torr TMA run. Note that for the Fickian and Berens-Hopfenberg models the fitting is done by visual

inspection for simplicity. The fit parameters for both models are provided in the SI Section S11. For the VPI system explored here, the reaction-diffusion model accounts for features missing from the oversimplified pure Fickian diffusion model and the polymer relaxation Berens-Hopfenberg model. A visual comparison reveals that the Berens-Hopfenberg model does better than the reaction-diffusion model in fitting the sorption process. However, the Berens-Hopfenberg model is simply fitting the total mass uptake to an exponential form (Section S3), and thus should be able to fit well to any sorption curve. Moreover, the Berens-Hopfenberg parameterization alone fails to explain the VPI process's underlying phenomena and as such is incapable of adequately predicting the desorption process in terms of both the residual mass and desorption rate. The Berens-Hopfenberg model is also incapable of providing information about the spatial distribution of mass uptake (i.e., depth profiles of precursor concentration) as this model only fits the overall mass uptake.

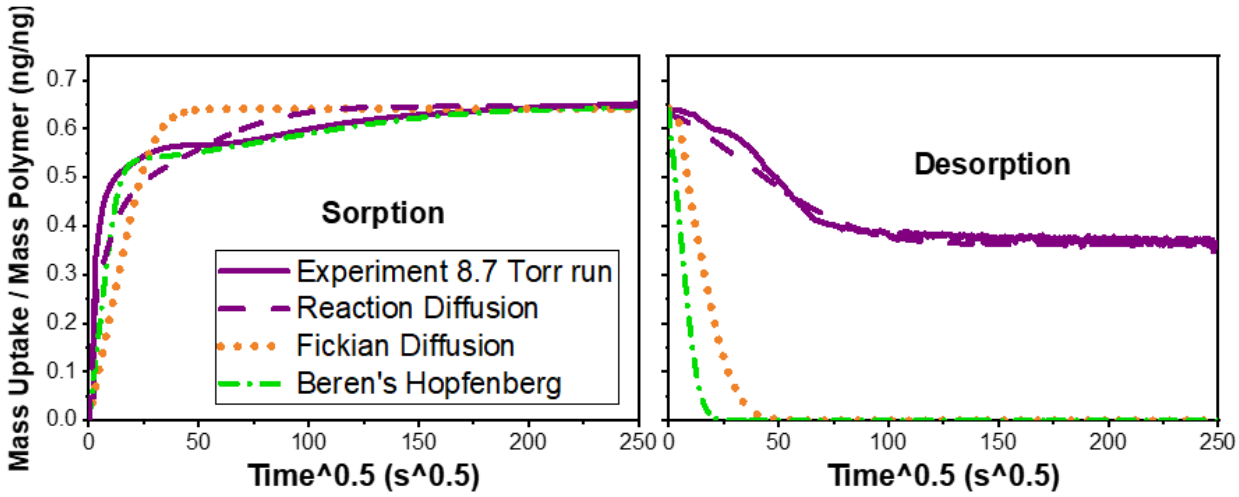

Figure 6. *Model comparison between Fickian, Berens Hopfenberg and our reaction-diffusion model for the TMA PMMA 8.7 Torr QCM experiment.*

4.5 Model Limitations

It is critical to point out some of the limitations of this reaction-diffusion transport model. One key assumption that is likely inaccurate is that polymer swelling and relaxation can be ignored. *In situ* spectroscopic ellipsometry studies performed on the infiltration of polystyrene (PS), PMMA, and P(S-r-MMA) with TMA at 90˚C (below the glass transition of PS and PMMA) clearly show thickness variations during the infiltration process.[38, 39] Generally, the contributions from polymer swelling and relaxation can be challenging to deconvolute from the contributions of reactions and diffusion. Incorporation of relaxation effects (e.g., a Berens-Hopfenberg-style approach) will no doubt improve the mathematical fitting of the model but incorporates additional physical parameters that are difficult to experimentally determine independently.

Another shortcoming is neglecting the likely significant role of heat. The sorption and reaction of TMA with PMMA is known to be exothermic, and thus heat should be released during the initial sorption stage. Heat release during sorption processes gives rise to well-known deviations from Fickian uptake responses via thermally-driven changes in diffusivity, sorption, and reaction rates. These effects can conceptually be accounted for via coupling of energy balances, but requires significant parameterization efforts to extract heats of reaction, sorption, and activation energies of diffusion. A third limiting assumption is that sorption is occurring via a linear isotherm. While Henry's Law makes for a physically representative starting point, the behaviors of the system are likely more complex and isotherm development is needed. Finally, the necessity of extracting the reaction rate constant and assuming a second order reaction is a limitation of this model. Unfortunately, the lack of literature on the reactions of TMA with PMMA necessitates this assumption.

While the phenomena of infiltrating the bulk of polymers with inorganics via vapor phase processes falls under the broad term VPI, several processing variations exist that include many

sequential pulses of precursors.[1, 37] These processes include sequential vapor infiltration (SVI), sequential infiltration synthesis (SIS), and multiple pulsed infiltration (MPI) or SIS in flow mode. The model proposed here is designed for and best applied to experiments consisting of a single precursor dose and exposure but can likely be further expanded to eventually explain processes that use multiple dose steps. Thermodynamically, a single long precursor exposure should produce an equivalent hybrid material to multiple, sequential metal-organic precursor exposures designed to maintain the same precursor pressure over time (e.g., an SVI process without continuous inert gas flow). The main difference is that for multiple doses and purges, free diffusing species will be desorbing during the purge step. If required, the model should be capable of capturing multiple short doses and purges by adjusting the sorption and desorption time to very short time intervals. The model is also likely capable of describing systems with multiple precursor (e.g., metal-organic) and co-reactant (e.g., oxidant) exposure cycles where the information from the end of the preceding cycle could be used as the starting point for the subsequent cycle (e.g., ALD on polymers or SIS). More challenging and currently largely unknown is the influence of having continuous inert gas purging during the VPI process (MPI, SVI). In fact, introducing a mixed nitrogen and precursor dose of varying overall pressure (primarily due to nitrogen content), has been shown to influence mass uptake in SVI.[14] While this model is a step towards better describing these complex processes, further study and even more sophisticated models are still needed.

5. Conclusions

In this work, a reaction-diffusion transport model for the vapor phase infiltration process is developed. This model captures changes in the diffusion process that result from reactions between the infiltrating precursors and polymer. The model is shown to both qualitatively and quantitatively capture and successfully predict VPI behaviors in an experimental case-study of the TMA-PMMA

VPI system. Importantly, this paper also uses nondimensionalization to generate a set of dimensionless numbers based on physical phenomena for the VPI process. Plotting the model using various sets of these dimensionless numbers provides insights into the types of transport and inorganic loading phenomena we can expect from a VPI process. Equations can also be solved to predict the spatial distribution of inorganic loading through the depth of the polymer. Overall, this work not only introduces a powerful new model capable of capturing the complexities of VPI, but also provides guidelines and a case-study of its utility in experimental parameterization and prediction. Importantly, these guidelines will allow the VPI community to standardize analysis and look for critical trends across systems. From this standardization and understanding, experiments designed to create specific structures and thereby properties can be developed. Analytical models such as the ones proposed here can also be integrated into process controllers, which provides a method for model-based control of emerging commercial VPI processes.

6. Supporting Information

The supporting information is free of charge at

Analysis of Leng's model; Fickian diffusion; Model assumptions; Boundary conditions for reaction-diffusion model; Non-dimensionalization of Fickian diffusion curves; Non-dimensionalization of the reaction-diffusion transport model for VPI; Definition of M_∞; Analysis of QCM data for experimental VPI runs; Full VPI experiments and pressure curves; Obtaining VPI parameters; Parameters for Fickian diffusion and Beren's Hopfenberg; Generating dimensionless numbers from 8.7 Torr run; nMAE calculation; Boundary Condition for Experiment

7. Acknowledgments

This material is based upon work supported by the National Science Foundation (DMREF-1921873). EKM was also supported by the Department of Defense (DoD) through the National Defense Science & Engineering Graduate Fellowship (NDSEG) Program. The authors would also like to thank Fengyi Zhang for the helpful discussions regarding the model development.

8. References

1. Leng, C. Z.; Losego, M. D., Vapor phase infiltration (VPI) for transforming polymers into organic-inorganic hybrid materials: a critical review of current progress and future challenges. *Mater. Horiz.* **2017,** *4* (5), 747-771.
2. Waldman, R. Z.; Mandia, D. J.; Yanguas-Gil, A.; Martinson, A. B. F.; Elam, J. W.; Darling, S. B., The chemical physics of sequential infiltration synthesis-A thermodynamic and kinetic perspective. *J. Chem. Phys.* **2019,** *151* (19), 190901.
3. Ingram, W. F.; Jur, J. S., Properties and Applications of Vapor Infiltration into Polymeric Substrates. *Jom* **2018,** *71* (1), 238-245.
4. Azpitarte, I.; Knez, M., Vapor phase infiltration: from a bioinspired process to technologic application, a prospective review. *Mrs Communications* **2018,** *8* (3), 727-741.
5. Subramanian, A.; Tiwale, N.; Nam, C.-Y., Review of Recent Advances in Applications of Vapor-Phase Material Infiltration Based on Atomic Layer Deposition. *Jom* **2018,** *71* (1), 185-196.
6. Losego, M. D.; Peng, Q., Atomic Layer Deposition and Vapor Phase Infiltration. *Surface Modification of Polymers* **2019**, 135-159.
7. Wang, W.; Chen, C.; Tollan, C.; Yang, F.; Beltran, M.; Qin, Y.; Knez, M., Conductive Polymer-Inorganic Hybrid Materials through Synergistic Mutual Doping of the Constituents. *ACS Appl Mater Interfaces* **2017,** *9* (33), 27964-27971.
8. Wang, W. K.; Chen, C. Q.; Tollan, C.; Yang, F.; Qin, Y.; Knez, M., Efficient and controllable vapor to solid doping of the polythiophene P3HT by low temperature vapor phase infiltration. *J. Mater. Chem. C* **2017,** *5* (10), 2686-2694.
9. Wang, W. K.; Yang, F.; Chen, C. Q.; Zhang, L. B.; Qin, Y.; Knez, M., Tuning the Conductivity of Polyaniline through Doping by Means of Single Precursor Vapor Phase Infiltration. *Adv. Mater. Interfaces* **2017,** *4* (4), 1600806-1600806.
10. Gregory, S. A.; Li, Y.; Monroe, T. D.; Li, J. J.; Yee, S. K.; Losego, M. D., Vapor Phase Infiltration Doping of the Semiconducting Polymer Poly(aniline) with TiCl4 + H2O: Mechanisms, Reaction Kinetics, and Electrical and Optical Properties. *ACS Applied Polymer Materials* **2021,** *3* (2), 720-729.
11. McGuinness, E. K.; Leng, C. Z.; Losego, M. D., Increased Chemical Stability of Vapor-Phase Infiltrated AlOx-Poly(methyl methacrylate) Hybrid Materials. *ACS Applied Polymer Materials* **2020,** *2* (3), 1335-1344.
12. McGuinness, E. K.; Zhang, F. Y.; Ma, Y.; Lively, R. P.; Losego, M. D., Vapor Phase Infiltration of Metal Oxides into Nanoporous Polymers for Organic Solvent Separation Membranes. *Chem. Mat.* **2019,** *31* (15), 5509-5518.
13. Akyildiz, H. I.; Lo, M.; Dillon, E.; Roberts, A. T.; Everitt, H. O.; Jur, J. S., Formation of novel photoluminescent hybrid materials by sequential vapor infiltration into polyethylene terephthalate fibers. *J. Mater. Res.* **2014,** *29* (23), 2817-2826.
14. Akyildiz, H. I.; Mousa, M. B. M.; Jur, J. S., Atmospheric pressure synthesis of photoluminescent hybrid materials by sequential organometallic vapor infiltration into polyethylene terephthalate fibers. *J. Appl. Phys.* **2015,** *117* (4), 7.
15. Akyildiz, H. I.; Stano, K. L.; Roberts, A. T.; Everitt, H. O.; Jur, J. S., Photoluminescence Mechanism and Photocatalytic Activity of Organic-Inorganic Hybrid Materials Formed by Sequential Vapor Infiltration. *Langmuir* **2016,** *32* (17), 4289-96.
16. Gong, B.; Peng, Q.; Jur, J. S.; Devine, C. K.; Lee, K.; Parsons, G. N., Sequential Vapor Infiltration of Metal Oxides into Sacrificial Polyester Fibers: Shape Replication and Controlled Porosity of Microporous/Mesoporous Oxide Monoliths. *Chem. Mat.* **2011,** *23* (15), 3476-3485.
17. Azpitarte, I.; Zuzuarregui, A.; Ablat, H.; Ruiz-Rubio, L.; Lopez-Ortega, A.; Elliott, S. D.; Knez, M., Suppressing the Thermal and Ultraviolet Sensitivity of Kevlar by Infiltration and Hybridization with ZnO. *Chem. Mater.* **2017,** *29* (23), 10068-10074.

18. Lee, S. M.; Pippel, E.; Gosele, U.; Dresbach, C.; Qin, Y.; Chandran, C. V.; Brauniger, T.; Hause, G.; Knez, M., Greatly increased toughness of infiltrated spider silk. *Science* **2009,** *324* (5926), 488-92.
19. Padbury, R. P.; Jur, J. S., Systematic study of trimethyl aluminum infiltration in polyethylene terephthalate and its effect on the mechanical properties of polyethylene terephthalate fibers. *J. Vac. Sci. Technol. A* **2015,** *33* (1), 9.
20. Berman, D.; Shevchenko, E., Design of functional composite and all-inorganic nanostructured materials via infiltration of polymer templates with inorganic precursors. *J. Mater. Chem. C* **2020,** *8* (31), 10604-10627.
21. Dusoe, K. J.; Ye, X.; Kisslinger, K.; Stein, A.; Lee, S. W.; Nam, C. Y., Ultrahigh Elastic Strain Energy Storage in Metal-Oxide-Infiltrated Patterned Hybrid Polymer Nanocomposites. *Nano. Lett.* **2017,** *17* (12), 7416-7423.
22. Ishchenko, O. M.; Krishnamoorthy, S.; Valle, N.; Guillot, J.; Turek, P.; Fechete, I.; Lenoble, D., Investigating Sequential Vapor Infiltration Synthesis on Block-Copolymer-Templated Titania Nanoarrays. *Journal of Physical Chemistry C* **2016,** *120* (13), 7067-7076.
23. Kamcev, J.; Germack, D. S.; Nykypanchuk, D.; Grubbs, R. B.; Nam, C. Y.; Black, C. T., Chemically enhancing block copolymers for block-selective synthesis of self-assembled metal oxide nanostructures. *ACS Nano* **2013,** *7* (1), 339-46.
24. Subramanian, A.; Doerk, G.; Kisslinger, K.; Yi, D. H.; Grubbs, R. B.; Nam, C. Y., Three-dimensional electroactive ZnO nanomesh directly derived from hierarchically self-assembled block copolymer thin films. *Nanoscale* **2019,** *11* (19), 9533-9546.
25. Tiwale, N.; Subramanian, A.; Kisslinger, K.; Lu, M.; Kim, J. Y.; Stein, A.; Nam, C. Y., Advancing next generation nanolithography with infiltration synthesis of hybrid nanocomposite resists. *J. Mater. Chem. C* **2019,** *7* (29), 8803-8812.
26. Yi, D. H.; Nam, C. Y.; Doerk, G.; Black, C. T.; Grubbs, R. B., Infiltration Synthesis of Diverse Metal Oxide Nanostructures from Epoxidized Diene-Styrene Block Copolymer Templates. *ACS Applied Polymer Materials* **2019,** *1* (4), 672-683.
27. Segal-Peretz, T.; Winterstein, J.; Doxastakis, M.; Ramirez-Hernandez, A.; Biswas, M.; Ren, J.; Suh, H. S.; Darling, S. B.; Liddle, J. A.; Elam, J. W.; de Pablo, J. J.; Zaluzec, N. J.; Nealey, P. F., Characterizing the Three-Dimensional Structure of Block Copolymers via Sequential Infiltration Synthesis and Scanning Transmission Electron Tomography. *ACS Nano* **2015,** *9* (5), 5333-47.
28. Segal-Peretz, T.; Zhou, C.; Ren, J. X.; Dazai, T.; Ocola, L. E.; Divan, R. N. S.; Nealey, P. F., Three Dimensional Assembly in Directed Self-assembly of Block Copolymers. *Journal of Photopolymer Science and Technology* **2016,** *29* (5), 653-657.
29. Obuchovsky, S.; Deckman, I.; Moshonov, M.; Peretz, T. S.; Ankonina, G.; Savenije, T. J.; Frey, G. L., Atomic layer deposition of zinc oxide onto and into P3HT for hybrid photovoltaics. *J Mater. Chem. C* **2014,** *2* (42), 8903-8910.
30. Obuchovsky, S.; Frankenstein, H.; Vinokur, J.; Hailey, A. K.; Loo, Y. L.; Frey, G. L., Mechanism of Metal Oxide Deposition from Atomic Layer Deposition inside Nonreactive Polymer Matrices: Effects of Polymer Crystallinity and Temperature. *Chem. Mater.* **2016,** *28* (8), 2668-2676.
31. Obuchovsky, S.; Shamieh, B.; Deckman, I.; Ankonina, G.; Frey, G. L., Harnessing ALD to directly map the morphology of organic photovoltaic bulk heterojunctions. *Sol. Energy Mater. Sol. Cells* **2015,** *143*, 280-283.
32. Padbury, R. P.; Jur, J. S., Effect of Polymer Microstructure on the Nucleation Behavior of Alumina via Atomic Layer Deposition. *J. Phys. Chem. C* **2014,** *118* (32), 18805-18813.
33. Sinha, A.; Hess, D. W.; Henderson, C. L., Area selective atomic layer, deposition of titanium dioxide: Effect of precursor chemistry. *Journal of Vacuum Science & Technology B* **2006,** *24* (6), 2523-2532.

34. Weisbord, I.; Shomrat, N.; Azoulay, R.; Kaushansky, A.; Segal-Peretz, T., Understanding and Controlling Polymer-Organometallic Precursor Interactions in Sequential Infiltration Synthesis. *Chem. Mater.* **2020,** *32* (11), 4499-4508.
35. Akyildiz, H. I.; Padbury, R. P.; Parsons, G. N.; Jur, J. S., Temperature and exposure dependence of hybrid organic-inorganic layer formation by sequential vapor infiltration into polymer fibers. *Langmuir* **2012,** *28* (44), 15697-704.
36. Padbury, R. P.; Jur, J. S., Temperature-dependent infiltration of polymers during sequential exposures to trimethylaluminum. *Langmuir* **2014,** *30* (30), 9228-38.
37. Padbury, R. P.; Jur, J. S., Comparison of precursor infiltration into polymer thin films via atomic layer deposition and sequential vapor infiltration using in-situ quartz crystal microgravimetry. *J Vac. Sci. Technol. A* **2014,** *32* (4), 041602-041602.
38. Caligiore, F. E.; Nazzari, D.; Cianci, E.; Sparnacci, K.; Laus, M.; Perego, M.; Seguini, G., Effect of the Density of Reactive Sites in P(S-r-MMA) Film during Al2O3 Growth by Sequential Infiltration Synthesis. *Adv. Mater. Interfaces* **2019,** *6* (12), 1900503.
39. Cianci, E.; Nazzari, D.; Seguini, G.; Perego, M., Trimethylaluminum Diffusion in PMMA Thin Films during Sequential Infiltration Synthesis: In Situ Dynamic Spectroscopic Ellipsometric Investigation. *Adv. Mater. Interfaces* **2018,** *5* (20), 1801016.
40. Leng, C. Z.; Losego, M. D., A physiochemical processing kinetics model for the vapor phase infiltration of polymers: measuring the energetics of precursor-polymer sorption, diffusion, and reaction. *Phys. Chem. Chem. Phys.* **2018,** *20* (33), 21506-21514.
41. Ito, S.; Ozaki, Y.; Nakamura, T.; Nakagawa, M., Depth profiles of aluminum component in sequential infiltration synthesis-treated electron beam resist films analyzed by time-of-flight secondary ion mass spectrometry. *Japanese Journal of Applied Physics* **2020,** *59* (SI), SIIC03.
42. Ozaki, Y.; Ito, S.; Hiroshiba, N.; Nakamura, T.; Nakagawa, M., Elemental depth profiles and plasma etching rates of positive-tone electron beam resists after sequential infiltration synthesis of alumina. *Japanese Journal of Applied Physics* **2018,** *57* (6), 06HG01.
43. Piercy, B. D.; Losego, M. D., Tree-based control software for multilevel sequencing in thin film deposition applications. *Journal of Vacuum Science & Technology B* **2015,** *33* (4), 043201-043201.
44. Akyildiz, H. I.; Jur, J. S., Organometallic exposure dependence on organic-inorganic hybrid material formation in polyethylene terephthalate and polyamide 6 polymer fibers. *J. Vac. Sci. Technol. A* **2015,** *33* (2), 5.
45. Sinha, A.; Hess, D. W.; Henderson, C. L., Transport behavior of atomic layer deposition precursors through polymer masking layers: Influence on area selective atomic layer deposition. *Journal of Vacuum Science & Technology B* **2007,** *25* (5), 1721-1728.
46. Thornton, A. W.; Nairn, K. M.; Hill, A. J.; Hill, J. M., New relation between diffusion and free volume: I. Predicting gas diffusion. *J. Membr. Sci.* **2009,** *338* (1-2), 29-37.
47. Davis, M. E.; Davis, R. J., *Fundamentals of Chemical Reaction Engineering*. McGraw-Hill: 2003; pp 219-220.
48. Fogler, H. S., *Elements of Chemical Reaction Engineering*. Prentice Hall PTR: 1999; pp 727.
49. Jones, A. A. D.; Jones, A. D., Numerical simulation and verification of gas transport during an atomic layer deposition process. *Materials Science in Semiconductor Processing* **2014,** *21*, 82-90.
50. Hanson, C. A.; Oldham, C. J.; Parsons, G. N., Paper deacidification and UV protection using ZnO atomic layer deposition. *J. Vac. Sci. Technol. A* **2012,** *30* (1), 01A117.
51. Jur, J. S.; Spagnola, J. C.; Lee, K.; Gong, B.; Peng, Q.; Parsons, G. N., Temperature-dependent subsurface growth during atomic layer deposition on polypropylene and cellulose fibers. *Langmuir* **2010,** *26* (11), 8239-44.
52. Jur, J. S.; Sweet, W. J.; Oldham, C. J.; Parsons, G. N., Atomic Layer Deposition of Conductive Coatings on Cotton, Paper, and Synthetic Fibers: Conductivity Analysis and Functional Chemical Sensing Using "All-Fiber" Capacitors. *Adv. Funct. Mater.* **2011,** *21* (11), 1993-2002.

53. Lee, K.; Jur, J. S.; Kim, D. H.; Parsons, G. N., Mechanisms for hydrophilic/hydrophobic wetting transitions on cellulose cotton fibers coated using Al2O3 atomic layer deposition. *J. Vac. Sci. Technol. A* **2012,** *30* (1), 01A163-01A163.
54. Li, Y.; Chen, L. H.; Wooding, J. P.; Zhang, F. Y.; Lively, R. P.; Ramprasad, R.; Losego, M. D., Controlling wettability, wet strength, and fluid transport selectivity of nanopaper with atomic layer deposited (ALD) sub-nanometer metal oxide coatings. *Nanoscale Advances* **2020,** *2* (1), 356-367.
55. Popescu, M. C.; Ungureanu, C.; Buse, E.; Nastase, F.; Tucureanu, V.; Suchea, M.; Draga, S.; Popescu, M. A., Antibacterial efficiency of cellulose-based fibers covered with ZnO and Al2O3 by Atomic Layer Deposition. *Applied Surface Science* **2019,** *481*, 1287-1298.
56. Short, A. E.; Pamidi, S. V.; Bloomberg, Z. E.; Li, Y.; Losego, M. D., Atomic layer deposition (ALD) of subnanometer inorganic layers on natural cotton to enhance oil sorption performance in marine environments. *J. Mater. Res.* **2019,** *34* (4), 563-570.
57. Wooding, J. P.; Li, Y.; Kalaitzidou, K.; Losego, M. D., Engineering the interfacial chemistry and mechanical properties of cellulose-reinforced epoxy composites using atomic layer deposition (ALD). *Cellulose* **2020,** *27* (11), 6275-6285.
58. Kim, S. W.; Rehman, M. M.; Sajid, M.; Rehman, M. M. U.; Gul, J.; Jo, J. D.; Choi, K. H., Encapsulation of polyvinyl alcohol based flexible temperature sensor through spatial atmospheric atomic layer deposition system to enhance its lifetime. *Thin Solid Films* **2019,** *673*, 44-51.
59. Spagnola, J. C.; Gong, B.; Arvidson, S. A.; Jur, J. S.; Khan, S. A.; Parsons, G. N., Surface and sub-surface reactions during low temperature aluminium oxide atomic layer deposition on fiber-forming polymers. *J. Mater. Chem.* **2010,** *20* (20), 4213-4222.
60. Dandley, E. C.; Needham, C. D.; Williams, P. S.; Brozena, A. H.; Oldham, C. J.; Parsons, G. N., Temperature-dependent reaction between trimethylaluminum and poly(methyl methacrylate) during sequential vapor infiltration: experimental and ab initio analysis. *J. Mater. Chem. C* **2014,** *2* (44), 9416-9424.
61. Hill, G. T.; Lee, D. T.; Williams, P. S.; Needham, C. D.; Dandley, E. C.; Oldham, C. J.; Parsons, G. N., Insight on the Sequential Vapor Infiltration Mechanisms of Trimethylaluminum with Poly(methyl methacrylate), Poly(vinylpyrrolidone), and Poly(acrylic acid). *Journal of Physical Chemistry C* **2019,** *123* (26), 16146-16152.
62. Biswas, M.; Libera, J. A.; Darling, S. B.; Elam, J. W., New Insight into the Mechanism of Sequential Infiltration Synthesis from Infrared Spectroscopy. *Chem. Mat.* **2014,** *26* (21), 6135-6141.
63. Berens, A. R.; Hopfenberg, H. B., Diffusion and Relaxation in Glassy Polymer Powders .2. Separation of Diffusion and Relaxation Parameters. *Polymer* **1978,** *19* (5), 489-496.
64. Berens, A. R.; Hopfenberg, H. B., Diffusion of Organic Vapors at Low Concentrations in Glassy Pvc, Polystyrene, and Pmma. *J. Membr. Sci.* **1982,** *10* (2-3), 283-303.

9. Table of contents graphic